mater.scichina.com link.springer.com

Published online 25 November 2022 | https://doi.org/10.1007/s40843-022-2251-8
Sci China Mater 2023, 66(3): 1071–1078

Atomically dispersed Pt in ordered PtSnZn intermetallic with Pt-Sn and Pt-Zn pairs for selective propane dehydrogenation

Chenliang Ye[1,2†], Mao Peng[3†], Yang Li[4], Dingsheng Wang[2], Chen Chen[2] and Yadong Li[2*]

ABSTRACT **With the surge of shale gas, propane dehydrogenation becomes increasingly important to synthesize propylene. Herein, a new type of ordered PtSnZn intermetallic clusters (~0.9 nm) supported on Al_2O_3 was synthesized by a stepwise approach including electrostatic adsorption and temperature-programmed reduction. The structure of the PtSnZn clusters results from a kinetically controlled process, and Pt atoms in the PtSnZn clusters are well isolated by Sn and Zn with Pt-Sn and Pt-Zn pairs. The PtSnZn/Al_2O_3 catalyst exhibits excellent catalytic performance for propane dehydrogenation, which achieves ~100% propylene selectivity and keeps a high propane conversion (>40%) during stability testing. The catalytic performance of PtSnZn/Al_2O_3 is also significantly higher than that of Pt/Al_2O_3, PtSn/Al_2O_3, and PtZn/Al_2O_3. Experiments and theoretical calculations indicate that the Sn 5p and Zn 4s orbitals are hybridized with Pt 5d by forming Pt-Sn and Pt-Zn pairs, which leads to the d band center of Pt deviating from Fermi level (−2.81 eV). The shift of the Pt d band center significantly decreases the adsorption energy of propylene and prohibits further dehydrogenation, resulting in high propylene selectivity and stability.**

Keywords: propane dehydrogenation, PtSnZn intermetallic cluster, atomically dispersed Pt

INTRODUCTION

Propylene has a large number of applications in chemical industries for producing downstream basic chemicals, such as acrylonitrile, propylene oxide, and polypropylene. With the surge of shale gas, propane dehydrogenation becomes increasingly important to synthesize propylene. At present, Pt-based catalysts are the most widely employed catalytic materials for light alkane dehydrogenation. Since the C–C bond cleavage is preferred to occur on agglomerated Pt particles, the catalytic performance of monometallic Pt catalysts is very poor [1–4]. It has been suggested that bimetallic catalysts, such as Pt-Sn, Pt-Zn, Pt-In, Pt-Ga, and Pt-Ge, are able to modify the geometric and electronic structure of Pt, so as to exhibit a higher catalytic performance than that of monometallic Pt catalysts [5–13]. However, there are still neighboring Pt–Pt bonds in these bimetallic catalysts, which would lead to C–C bond cleavage and generate cokes easily during catalytic dehydrogenation.

Single atomic site catalysts have attracted great attention in recent years due to their minimum ensembles and unique electronic structure [14–24]. Alloys with atomically dispersed active sites (AADAS) are one of the special catalytic materials with isolated active metals anchored in the hosting metals. According to the atomic arrangement, alloys can be classified into solid solutions and intermetallic compounds [25]. Solid solutions contain metals that randomly substitute the atomic positions of the parent metal, while intermetallic compounds possess a uniform crystal structure and highly ordered atomic distribution [26–29]. It has been suggested that AADAS of solid solutions exhibit a higher selectivity of C–H bond cleavage than that of traditional bimetallic catalysts with Pt/Cu being a successful example [30,31]. However, under severe reaction conditions, it is a great challenge to stabilize the structure of solid solutions and keep high catalytic selectivity. Intermetallic compounds also have a potential to serve as AADAS, since the ensembles of active metals can be reduced by the neighboring promoter metals. More importantly, the atomic arrangement of intermetallic compounds is more ordered than that of solid solutions, which is beneficial for controlling the particle sizes and achieving high thermodynamic stability under severe catalytic conditions [32–35]. The AADAS of ordered active sites in intermetallic clusters (<1 nm) is promising to display a higher selectivity and stability for propane dehydrogenation than that of AADAS in large solid solutions.

Herein, we prepared an ordered PtSnZn intermetallic compound with Al_2O_3 as the support (PtSnZn/Al_2O_3) by a stepwise approach including electrostatic adsorption and temperature-programmed reduction (TPR). The particle sizes of the PtSnZn intermetallic compound are at cluster scale (~0.9 nm), and the Pt atoms are well isolated by Sn and Zn. The PtSnZn/Al_2O_3 catalyst exhibits high selectivity and stability for propane dehydrogenation, which is significantly better than that of Pt/Al_2O_3, PtSn/Al_2O_3 and PtSnZn/Al_2O_3. Our work has revealed that, by forming Pt-Sn and Pt-Zn pairs in the PtSnZn intermetallic clusters, the d band center of Pt shifts to a lower value of Fermi level (−2.81 eV), which significantly decreases the adsorption energy of propylene and prohibits further dehy-

[1] College of Physics and Optoelectronic Engineering, Shenzhen University, Shenzhen 518060, China
[2] Department of Chemistry, Tsinghua University, Beijing 100084, China
[3] School of Chemical Engineering and Technology, Tianjin University, Tianjin 300072, China
[4] Beijing Single-atom Catalysis Technology Co., Ltd., Beijing 100094, China
† These authors contributed equally to this work.
* Corresponding author (email: ydli@mail.tsinghua.edu.cn)

drogenation, leading to high propylene selectivity and stability.

EXPERIMENTAL SECTION

Synthesis of the catalysts

The $PtSnZn/Al_2O_3$ sample was prepared by a stepwise approach including electrostatic adsorption and TPR. Briefly, 0.014 g of $ZnCl_2$ and 0.023 g of $SnCl_2{\cdot}2H_2O$ were dissolved in 0.4 mL of methanol, which was then added dropwise to 1 g of Al_2O_3. The acquired $SnZn/Al_2O_3$ was dried overnight at 100°C and calcined at 550°C for 3 h. Then 0.053 g of $H_2PtCl_6{\cdot}6H_2O$ was dissolved in 0.37 mL of water, and 0.03 mL of hydrochloric acid (37% HCl) was added to the solution to enrich the H^+ concentration. The solution was added dropwise to the prepared $SnZn/Al_2O_3$. This catalyst was then dried overnight at 125°C and calcined at 225°C for 3 h. Finally, the catalyst was reduced in 5% H_2/N_2 at 150°C for 10 min, 200°C for 30 min, 250°C for 10 min, and 550°C for 30 min. For comparison, Pt/Al_2O_3, $PtSn/Al_2O_3$, and $PtZn/Al_2O_3$ catalysts with the same Pt, Sn, and Zn loadings as that of $PtSnZn/Al_2O_3$ were also synthesized by the similar procedure.

Characterizations and catalytic testing

Scanning transmission electron microscopy (STEM) was carried out using Titan 80-300 scanning/transmission electron microscope operated at 300 kV with a high angle annular dark field (HAADF). The particle size distribution was obtained by calculating 1000 particles for each sample. The inductively coupled plasma optical emission spectrometry (ICP-OES) was conducted on an Agilent-5110 equipment. X-ray diffraction (XRD) was performed on a Rigaku RU-200b with Cu Kα radiation. The theoretical diffraction patterns of the PtSnZn intermetallic were acquired with materials analysis using diffraction. The X-ray photoelectron spectroscopy (XPS) experiments were performed at an ESCALAB 250Xi, ThermoFischer. The X-ray was from Al Kα ($h\nu$ = 1486.6 eV) operated at 12.5 kV. The thermogravimetric analysis (TGA) was carried out on a SDT Q600 V20.9 Build 20 instrument using the differential scanning calorimetry (DSC)-TGA standard module. The temperature was increased from 35 to 800°C in the air with a heating rate of 10°C min^{-1}. N_2 physisorption measurement was performed by a Quantachrome Instrument of version 3.01 at 77 K. The Pt L_3 edge extended X-ray absorption find structure (EXAFS) spectroscopy was collected on the 1W1B station at Beijing Synchrotron Radiation Facility (BSRF) using a transmission mode. The Pt foil was employed to calibrate the energy and calculate the amplitude reduction factor (S_0^2). TPR was performed on the AutoChem II 2920 V5.02. *In situ* infrared spectroscopy of chemisorbed CO was collected from a Nicolet 6700 FT-IR spectrometer. The catalytic testing of propane dehydrogenation was performed in a fixed-bed quartz tube reactor. The reaction temperature was 500°C and the reactants were 5% C_3H_8 balanced with N_2. The gas hourly space velocity (GHSV) was adjusted to determine the selectivity at a certain conversion. The propylene selectivity of this work was based on gas phase selectivity. For stability testing, the usage of catalysts was 0.4 g, and the flow rate of 5% C_3H_8 was 20 mL min^{-1}.

Theoretical calculations

The Vienna *ab initio* Simulation Package was applied to carry out the DFT calculations. The transition state of every elementary reaction was obtained by the climbing-image nudged elastic band (CI-NEB) method and the dimer method. Vibrational frequency was calculated to estimate the accuracy of transition states, and weak van der Waals interactions were included to correctly describe the physisorption. Pt, PtSn, PtZnSn, and PtZn clusters-loaded $Al_2O_3(211)$ surface model were constructed to explore the role of isolated Pt atom in the selectivity of propane dehydrogenation. $Al_2O_3(211)$ was modeled by using a $p(2 \times 1)$ supercell with four O-Al layers; the bottom one O-Al layer was fixed and other O-Al layers with loaded clusters were relaxed. Pt(111) was constructed with a $p(4 \times 4)$ supercell and three atomic layers; during calculation, the bottom one layer was fixed and the others relaxed. For PtSn(110), PtZnSn(110), and PtZn (110), a $p(2 \times 2)$ supercell with three atomic layers was constructed; the bottom one layer was fixed and others relaxed. The vacuum slab was 15 Å in the z direction.

The adsorption energy (E_{ads}) of species was calculated as follows:

$$E_{ads} = E_{adsorbate/slab} - E_{slab} - E_{adsorbate}, \quad (1)$$

where $E_{adsorbate/slab}$ is the total energy of the adsorbate and catalyst; E_{slab} is the energy of the catalyst; $E_{adsorbate}$ is the energy of the isolated molecule in the gas phase.

The activation barrier (E_a) and reaction energy (ΔH) were calculated using the following equations:

$$E_a = E_{TS} - E_R, \quad (2)$$

$$\Delta H = E_p - E_R, \quad (3)$$

where E_R, E_{TS}, and E_P are the total energies of reactant, transition state, and product for the reaction, respectively.

RESULTS AND DISCUSSION

Pt-Sn-Zn trimetallic catalyst supported on γ-Al_2O_3 was synthesized by a stepwise approach including electrostatic adsorption and TPR. The crystal size of the Al_2O_3 is very small, only ~15 nm, which plays a key role to acquire highly dispersed metal precursors (Fig. S1). $SnCl_2$ and $ZnCl_2$ were dissolved in methanol and dropwise added to the Al_2O_3, and then calcinated at 550°C to obtain $SnZnO_x/Al_2O_3$. Hydrochloric acid was added to the H_2PtCl_4 solution to enrich the H^+ concentration, and the obtained solution was added dropwise to $SnZnO_x/Al_2O_3$. The solution is sufficiently acidified to adsorb $[PtCl_4]^{2-}$ on the Al_2O_3 surface, which induces strong electrostatic adsorption of negatively charged $[PtCl_4]^{2-}$ to the oppositely charged Al_2O_3 surface [36]. The precursor was calcinated at 225°C for 3 h to form PtO_x on $SnZnO_x/Al_2O_3$. Finally, the sample was reduced at around 200°C to obtain metallic Pt, followed by reduction at 550°C to obtain Pt-Sn-Zn trimetallic particles. For comparison, Pt/Al_2O_3, $PtSn/Al_2O_3$, and $PtZn/Al_2O_3$ were also synthesized by the similar process (Table S1, Figs S2 and S3). The surface area and average pore diameter of $PtSnZn/Al_2O_3$ are 90 m^2 g^{-1} and 6.2 nm respectively, which are close to those of Pt/Al_2O_3, $PtSn/Al_2O_3$, and $PtZn/Al_2O_3$ (Fig. 1a, b). As shown in Fig. 1c, d, the particles are well dispersed on the Al_2O_3 with an average size of 0.9 nm. We further conducted electron dispersive spectroscopy (EDS) to analyze the element compositions of $PtSnZn/Al_2O_3$. As displayed in Fig. 1e, Fig. S4, and Table S2, the mapping areas of Pt, Sn, and Zn are almost overlapped, indicating the formation of PtSnZn trimetallic alloys.

To identify the precise structure of the PtSnZn cluster, Pt L_3 edge EXAFS spectroscopy was carried out to characterize the coordinated environments of Pt. As displayed in Fig. 2a, the

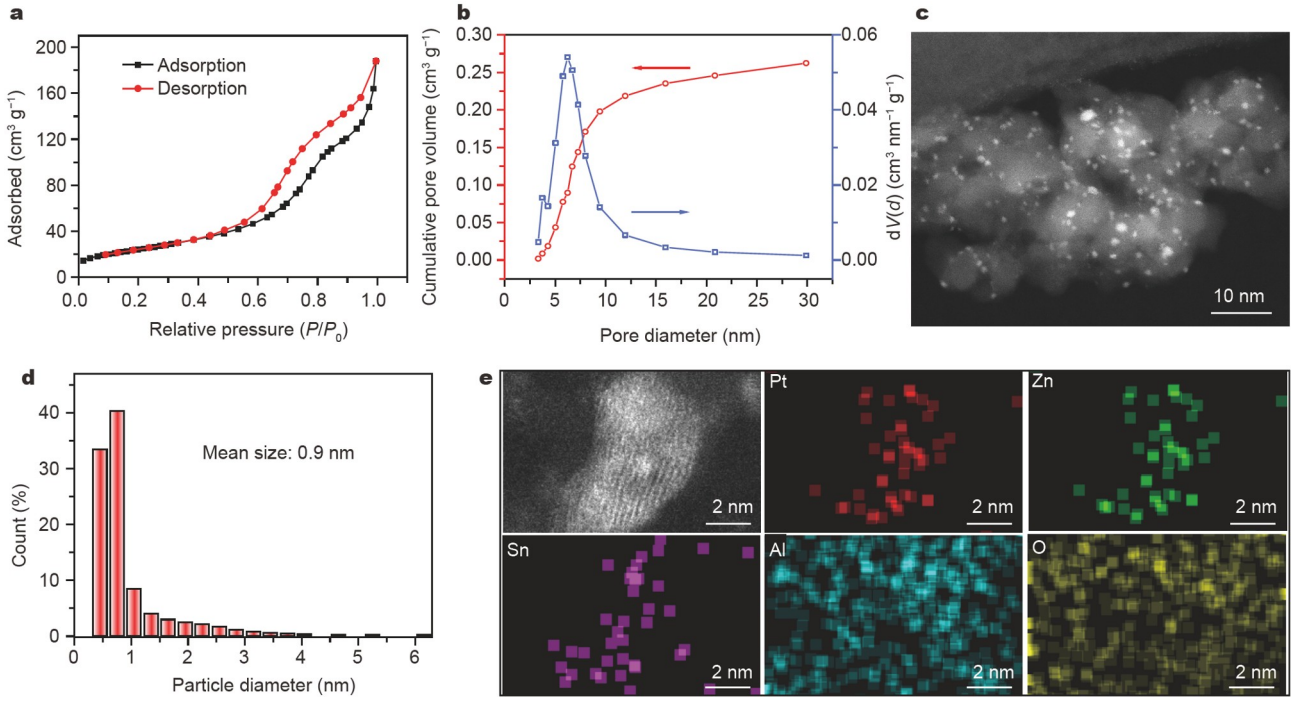

Figure 1 Nitrogen sorption isotherm and spherical aberration-corrected HAADF STEM of PtSnZn/Al_2O_3. (a) Nitrogen sorption isotherm; (b) pore size distribution; (c, d) sample image and particle size distribution; (e) EDS mapping.

Pt/Al_2O_3 sample shows three main peaks from 1.7 to 3.2 Å in the R-space Fourier transform EXAFS, which is attributed to the Pt–Pt scattering of the first nearest shell. The Pt–Pt scattering peaks are not observed in the PtSnZn/Al_2O_3 sample, indicating that the Pt atoms are isolated by Sn, Zn, or O from Al_2O_3. These results are also confirmed by the wavelet transforms (WT). As shown in Fig. 2b, c, the intensity maxima of PtSnZn/Al_2O_3 is far away from that of Pt/Al_2O_3, suggesting the disappearance of Pt–Pt bonds in PtSnZn/Al_2O_3. The R-space Fourier transform EXAFS of PtSnZn/Al_2O_3 was fitted to obtain the quantitative local structure of Pt. As shown in Fig. 2d, Figs S5–S7 and Table S3, the Pt atoms are well isolated by Sn and Zn with Pt-Sn and Pt-Zn coordination numbers at 2.0 and 2.3 respectively, indicating the formation of trimetallic alloys, which is consistent with the EDS results. In addition, there are Pt–O bonds in PtSnZn/Al_2O_3, which could be attributed to the surface oxidized Pt species. The partial oxidization phenomenon is also observed in the Sn and Zn species (Fig. S8).

To identify the long-range ordered structure of the PtSnZn alloy, we carried out XRD analysis on the samples. As illustrated in Fig. 2e, the XRD patterns of Pt/Al_2O_3, PtSn/Al_2O_3, PtZn/Al_2O_3, and PtSnZn/Al_2O_3 are almost the same, which are identical to that of Al_2O_3. This phenomenon results from low Pt loadings (~1.5%), small particle sizes and strong diffraction peaks of the background (Al_2O_3). To address this issue, we prepared Pt-Sn-Zn catalyst with large particle sizes by increasing the calcination temperature to 550°C before reduction (namely PtSnZn/Al_2O_3-550). The particle size of PtSnZn/Al_2O_3-550 is ~6 nm (Fig. S9). Interestingly, four new diffraction peaks with very weak intensity appear at 2θ of 25°, 30°, 42°, and 44° (Fig. 2f). XRD simulation results suggest that the four diffraction peaks are attributed to the ordered PtSnZn intermetallic compound of hexagonal structure, in which the shortest Pt–Pt distance is 4.009 Å (Table S4, Fig. S10). The shortest Pt–Pt distance in the PtSnZn intermetallic compound is significantly longer than that of monometallic Pt (2.77 Å). The long Pt–Pt distance results from the Sn and Zn that isolate Pt atoms, which is consistent with the EXAFS analysis. However, the Pt-Sn and Pt-Zn coordination numbers from EXAFS are significantly lower than those of standard bulk PtSnZn intermetallic compound, which results from the high ratio of surface unsaturated atoms of small particles. Notably, the crystal structures of PtSnZn/Al_2O_3-550 and PtSnZn/Al_2O_3 may not the same, since their calcination temperatures are different and the reduction process can change the valence of Pt (Fig. S11). We further compared the q-space EXAFS of PtSnZn/Al_2O_3-550 and PtSnZn/Al_2O_3. As displayed in Fig. 2g, except for the intensity, the oscillations of the two samples are almost identical, indicating the calcination temperature does not have a significant effect on the crystal structure of the PtSnZn intermetallic compound.

The STEM, EXAFS, and XRD results demonstrate an ordered PtSnZn intermetallic cluster supported on Al_2O_3. The phase diagram is regularly applied to guide the synthesis and predict the potential structure of alloys. In the phase diagram, the formation of bulk alloys requires a high temperature to melt and mix all the metals. All atoms freely move in the melt and a cooling thermodynamically stable structure is formed later. The formation of the small cluster by H_2 reduction is quite different from that of bulk alloys. As shown in the H_2-TPR analysis (Fig. 2h), PtO_x in Pt/Al_2O_3 is fully reduced to metallic Pt from 200 to 300°C. In the PtSnZn/Al_2O_3 catalyst, PtO_x is firstly reduced to metallic Pt at a low temperature and then the $SnZnO_x$ near to Pt is reduced by a hydrogen spilled over from Pt at a higher temperature to form PtSnZn intermetallic. The structure of PtSnZn intermetallic compound is determined by the diffusion of Sn and Zn into Pt, which is a kinetically controlled process. These results were also confirmed by the *in situ* infrared spectroscopy of chemisorbed CO. As shown in Fig. 2i, both

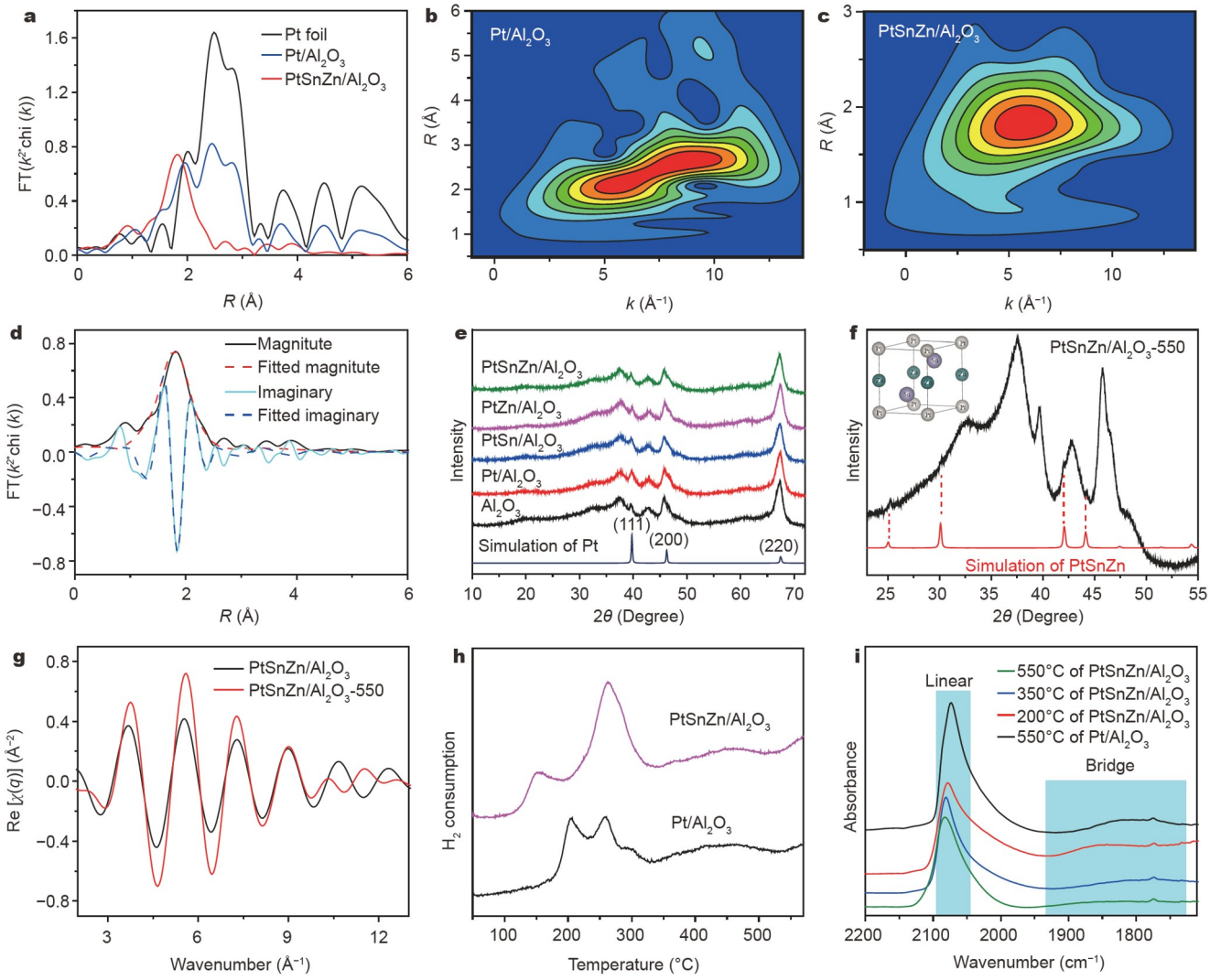

Figure 2 Structure identification of the samples. (a) R-space EXAFS of the samples; (b, c) WT of Pt/Al_2O_3 and $PtSnZn/Al_2O_3$; (d) EXFAS fitting spectrum of $PtSnZn/Al_2O_3$; (e, f) XRD patterns of the samples; (g) q-space EXAFS of $PtSnZn/Al_2O_3$ and $PtSnZn/Al_2O_3$-550; (h) H_2-TPR of Pt/Al_2O_3 and $PtSnZn/Al_2O_3$; (i) *In situ* infrared spectroscopy of chemisorbed CO.

linearly adsorbed CO (1990–2100 cm^{-1}) and bridge bound CO (1720–1900 cm^{-1}) appear in the fully reduced Pt/Al_2O_3 sample. The bridge bound CO results from the surface ensembles of multiple Pt atomic neighbors [37–40]. The infrared spectroscopy of $PtSnZn/Al_2O_3$ reduced at 200°C is similar to that of Pt/Al_2O_3, suggesting the formation of metallic Pt. When the reduction temperature increases to 350°C, the bridge bound CO of $PtSnZn/Al_2O_3$ becomes weaker, indicating that partial Sn and Zn atoms diffuse into Pt particles. Further increasing the reduction temperature to 550°C, the bridge bound CO almost disappear, suggesting that ensembles of Pt atoms are significantly reduced.

The catalytic performance of the samples was tested in a fixed bed reactor. Since the carbon balance of the samples is higher than 97%, the propylene selectivity of this work is based on gas phase selectivity (Table S5). As shown in Fig. 3a, at 10% propane conversion, the propylene selectivity of Pt/Al_2O_3 is ~92%. The propylene selectivity decreases to ~64% when the propane conversion increases to 50%. The propylene selectivity of $PtSn/Al_2O_3$ and $PtZn/Al_2O_3$ is also influenced by the propane conversion. At 15% propane conversion, the propylene selectivity of $PtSn/Al_2O_3$ and $PtZn/Al_2O_3$ is higher than 93%, and it decreases very quickly with increasing propane conversion. For $PtSnZn/Al_2O_3$, the sample keeps ~100% propylene selectivity even though the propane conversion increases to ~50%. We further investigated the catalytic stability of the catalysts. As displayed in Fig. 3b, the propane conversion of Pt/Al_2O_3 drops very quickly, which decreases from 57% to 4.5% within 200 min, while the $PtSnZn/Al_2O_3$ catalyst keeps a high propane conversion after 720 min testing (>40%). The stability and turnover frequency (TOF) of $PtSnZn/Al_2O_3$ catalyst are also significantly higher than that of $PtSn/Al_2O_3$ and $PtZn/Al_2O_3$ (Fig. S12 and Table S6). Under very high space velocity (23.6 h^{-1}) with pure C_3H_8 as the feedstock, the $PtSnZn/Al_2O_3$ catalyst also exhibits a high propylene selectivity (~99%) and stability (Fig. S13). Notably, although the propylene selectivity and stability of the $PtSnZn/Al_2O_3$ catalyst are excellent, the regeneration properties of this catalyst still need to be improved (Table S7).

Coke deposition during propane dehydrogenation is viewed as the main reason for deactivation. To investigate the coke deposition on the spent catalysts, we carried out TGA on Pt/

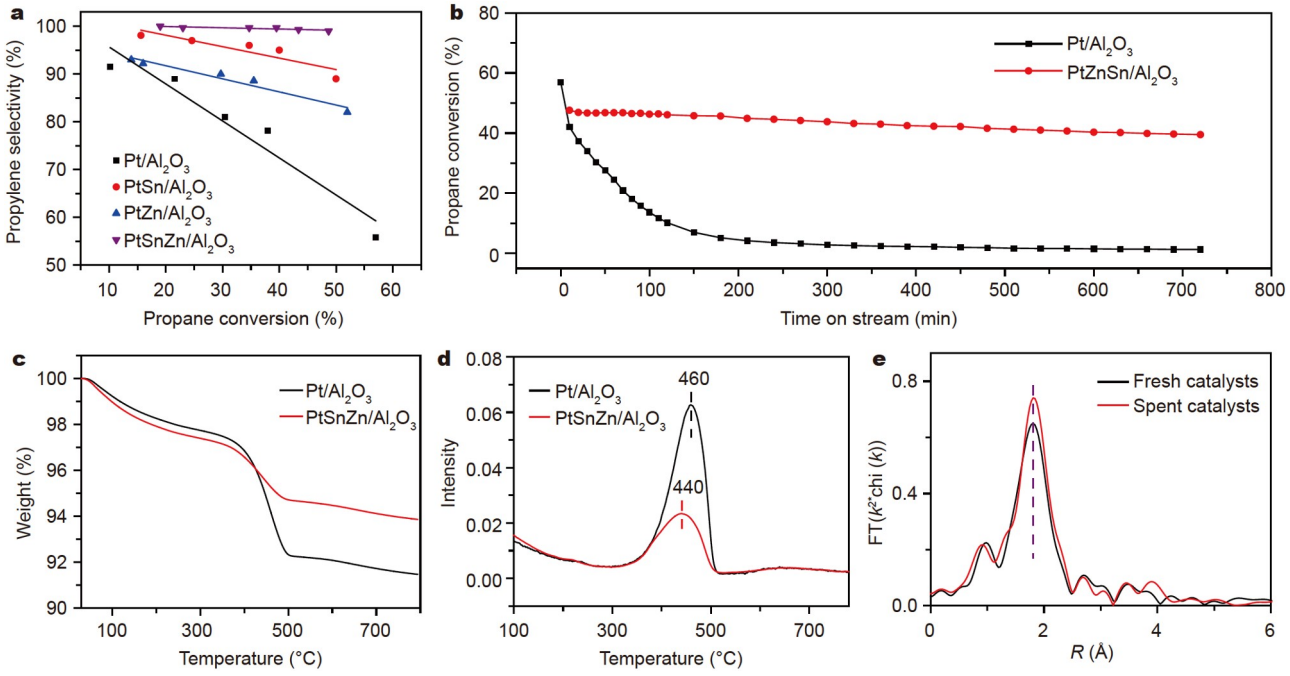

Figure 3 Catalytic performance and deactivation studies of the samples. (a) Propylene selectivity at different propane conversions; (b) stability testing of Pt/Al_2O_3 and $PtSnZn/Al_2O_3$; (c) TGA; (d) DTGA; (e) R-space EXAFS of the fresh $PtSnZn/Al_2O_3$ and the spent $PtSnZn/Al_2O_3$.

Al_2O_3 and $PtSnZn/Al_2O_3$ of the spent catalysts. As shown in Fig. 3c, when the temperature is raised to 800°C in air, the total weight losses of Pt/Al_2O_3 and $PtSnZn/Al_2O_3$ are ~9% and ~6%, respectively. The weight losses can be classified into two steps as evidenced by derivative TGA (DTGA) (Fig. 3d). The weight losses before 300°C are attributed to evaporation of absorbed water, while the weight losses between 300 and 500°C result from the decomposition of cokes [41]. The weight of cokes in the spent Pt/Al_2O_3 is 5.4%, while that in the spent $PtSnZn/Al_2O_3$ is only 2.5%. It is well known that the derivative thermogravimetric peak at high temperatures correlates with stable carbon species like graphitic carbon [42,43]. The derivative thermogravimetric peak position of $PtSnZn/Al_2O_3$ (440°C) is lower than that of Pt/Al_2O_3 (460°C), which means the carbon species on $PtSnZn/Al_2O_3$ are easier to be removed during catalytic dehydrogenation than those on Pt/Al_2O_3. We further investigated the potential structure change of $PtSnZn/Al_2O_3$ after stability testing. As shown in Fig. 3e, the Pt L_3 edge R-space EXAFS of the spent catalyst is compared with that of the fresh catalyst. The scattering peak position of the spent catalyst is identical to that of the fresh catalyst (1.82 Å), indicating the bond distance of the spent catalyst is the same as that of the fresh catalyst, which means the structure of PtSnZn intermetallic is not destroyed under severe reaction conditions.

DFT calculations provide insights into the high catalytic performance of $PtZnSn/Al_2O_3$ for propane dehydrogenation. We constructed models of Pt, PtSn, PtZn, and PtSnZn clusters anchored on Al_2O_3 (Fig. 4a–d, Tables S8 and S9). According to the identified structure, the Pt atoms in $PtZnSn/Al_2O_3$ are isolated by neighboring Zn and Sn atoms. The electronic structure of Pt is significantly influenced by the unique geometric structure. As shown in Fig. 4e–h, Zn 4s and Sn 5p orbitals are hybridized with Pt 5d, which leads to the d band center of Pt deviating from the Fermi level. The d-band center of surface Pt downshifts from −1.40 to −1.90, −2.41, and −2.81 eV on Pt/Al_2O_3, $PtZn/Al_2O_3$, $PtSn/Al_2O_3$, and $PtSnZn/Al_2O_3$, respectively (Table S10). Propylene desorption is viewed as the vital process for propane dehydrogenation, since the high adsorption energy of propylene on the catalysts would lead to further dehydrogenation and generate cokes [44]. The electronic interaction of Pt-Sn and Pt-Zn limits the charge transfer between Pt and propylene, which would weaken the adsorption of propylene and facilitate propylene desorption. We further calculated the potential energy for propane dehydrogenation on Pt/Al_2O_3, $PtZn/Al_2O_3$, $PtSn/Al_2O_3$, and $PtSnZn/Al_2O_3$ (Fig. 4i, Tables S11–S13, Figs S14–S23). The propylene selectivity is influenced by both propylene adsorption energy and the energy difference between propylene desorption and propylene dehydrogenation; the lower propylene adsorption energy and the more negative value of the energy difference would lead to higher propylene selectivity. The propylene adsorption energy of $PtSnZn/Al_2O_3$ (−28.2 kJ mol^{-1}) is higher than that of Pt/Al_2O_3 (−159.9 kJ mol^{-1}), $PtSn/Al_2O_3$ (−68.8 kJ mol^{-1}) and $PtZn/Al_2O_3$ (−112.1 kJ mol^{-1}). Meanwhile, among the four catalysts, $PtSnZn/Al_2O_3$ exhibits the highest negative value (−192.7 kJ mol^{-1}) of the energy difference between propylene desorption and propylene dehydrogenation. We also investigated the potential energy on Pt(111), PtZn(110), PtSn(110), and PtSnZn(110), which can represent larger particles. As shown in Fig. 4j, PtSnZn(110) exhibits a higher negative value (−55.1 kJ mol^{-1}) of the energy difference between propylene desorption and propylene dehydrogenation than that of Pt(111) (58.4 kJ mol^{-1}), PtSn(110) (−29.0 kJ mol^{-1}), and PtZn(110) (−10.8 kJ mol^{-1}). Moreover, it also illustrates that the small cluster of $PtSnZn/Al_2O_3$ would have a higher propylene selectivity than that of PtSnZn(110) (−192.7 & −55.1 kJ mol^{-1}).

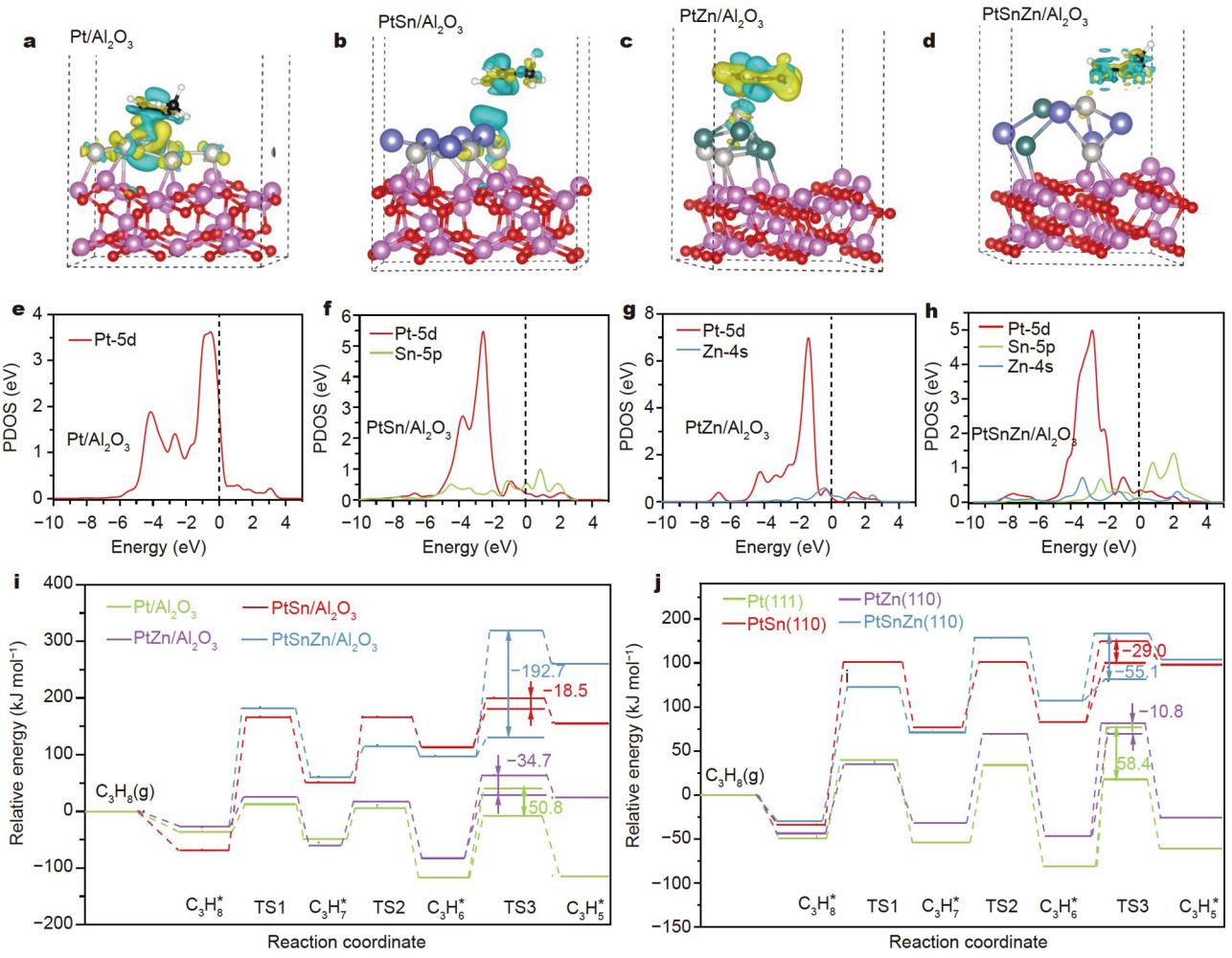

Figure 4 DFT calculation results. (a–d) Structure models of the samples; (e–h) the partial density of states (PDOS); (i) the potential energies of the cluster models; (j) the potential energies of the crystal phase models.

This work illustrates that isolating Pt atoms with Pt-Sn and Pt-Zn pairs in PtSnZn intermetallic clusters is an effective way to modify the geometric and electronic structure of Pt for propane dehydrogenation. For geometric structure, it has been suggested that hydrogenolysis and carbon deposits need to be in the vicinity of adsorbed hydrogen, which is more likely to occur on large Pt ensembles than on small particles [44,45]. Sun *et al.* [31] have reported a Pt-Cu/Al_2O_3 catalyst with atomically dispersed Pt in Cu (~10 nm solid solution), which achieves a high propylene selectivity (~90%) for propane dehydrogenation. Cybulskis *et al.* [46] have illustrated that a Pt-Zn intermetallic compound with the Pt_1Zn_1 tetragonal structure exhibits a high ethylene selectivity for ethane dehydrogenation; they speculated that the high catalytic performance results from the reduced Pt ensembles with Pt–Zn bonds in the tetragonal structure. In addition to the geometric effects, alloys also have the potential to modify the electronic structure of Pt, so as to improve the catalytic performance. It has been suggested that low-electronegativity elements, such as Sn and Zn, are able to transfer electrons to the 5d band of Pt atoms, which would alter the adsorptive properties and improve the catalytic selectivity [47–49]. In recent years, it has been reported that adding rare-earth elements is also able to modify the geometric and electronic structure of Pt for light alkane dehydrogenation. Ryoo *et al.* [50] synthesized rare-earth-platinum intermetallic nanoparticles supported on a mesoporous zeolite that has pore walls with surface framework defects. The Pt_3La intermetallic nanoparticles show a high initial propane conversion of 40%, and display a high propylene selectivity (~97%) and stability. For our PtSnZn intermetallic compound, the Pt atoms are isolated by Sn and Zn in ultrasmall clusters (~0.9 nm), and the Zn 4s and Sn 5p orbitals are hybridized with Pt 5d by forming Pt-Sn and Pt-Zn pairs, leading to the d band center of Pt deviating from the Fermi level. The optimized geometric and electronic structure results in high propylene selectivity and stability for propane dehydrogenation.

CONCLUSIONS

In summary, a kind of PtSnZn intermetallic clusters (~0.9 nm) supported on Al_2O_3 was synthesized by a stepwise approach including electrostatic adsorption and TPR. The PtSnZn intermetallic clusters possess well isolated Pt atoms by forming Pt-Sn and Pt-Zn pairs. Due to the unique structure, the PtSnZn/Al_2O_3 catalyst shows a significantly higher catalytic performance than that of Pt/Al_2O_3, PtSn/Al_2O_3, and PtZn/Al_2O_3 for propane dehydrogenation, which achieves ~100% propylene selectivity and high stability. Our work has revealed that, the Sn 5p and Zn 4s orbitals are hybridized with Pt 5d, and the d band center of Pt deviating from the Fermi level (−2.81 eV), which significantly

decreases the adsorption energy of propylene and limits further dehydrogenation, resulting in the high catalytic performance.

Received 16 June 2022; accepted 12 September 2022; published online 25 November 2022

1 Ye C, Wu Z, Liu W, *et al.* Structure determination of a surface tetragonal Pt_1Sb_1 phase on Pt nanoparticles. Chem Mater, 2018, 30: 4503–4507
2 Bariås OA, Holmen A, Blekkan EA. Propane dehydrogenation over supported Pt and Pt-Sn catalysts: Catalyst preparation, characterization, and activity measurements. J Catal, 1996, 158: 1–12
3 Jablonski EL, Castro AA, Scelza OA, *et al.* Effect of Ga addition to Pt/Al_2O_3 on the activity, selectivity and deactivation in the propane dehydrogenation. Appl Catal A-Gen, 1999, 183: 189–198
4 Wang LC, Zhang Y, Xu J, *et al.* Non-oxidative dehydrogenation of ethane to ethylene over ZSM-5 zeolite supported iron catalysts. Appl Catal B-Environ, 2019, 256: 117816
5 Motagamwala AH, Almallahi R, Wortman J, *et al.* Stable and selective catalysts for propane dehydrogenation operating at thermodynamic limit. Science, 2021, 373: 217–222
6 Rochlitz L, Searles K, Alfke J, *et al.* Silica-supported, narrowly distributed, subnanometric Pt-Zn particles from single sites with high propane dehydrogenation performance. Chem Sci, 2020, 11: 1549–1555
7 Yan H, He K, Samek IA, *et al.* Tandem In_2O_3-Pt/Al_2O_3 catalyst for coupling of propane dehydrogenation to selective H_2 combustion. Science, 2021, 371: 1257–1260
8 Fan X, Li J, Zhao Z, *et al.* Dehydrogenation of propane over PtSnAl/SBA-15 catalysts: Al addition effect and coke formation analysis. Catal Sci Technol, 2015, 5: 339–350
9 Ingale P, Knemeyer K, Preikschas P, *et al.* Design of PtZn nanoalloy catalysts for propane dehydrogenation through interface tailoring *via* atomic layer deposition. Catal Sci Technol, 2021, 11: 484–493
10 Shen LL, Xia K, Lang WZ, *et al.* The effects of calcination temperature of support on PtIn/Mg(Al)O catalysts for propane dehydrogenation reaction. Chem Eng J, 2017, 324: 336–346
11 Wang P, Yao J, Jiang Q, *et al.* Stabilizing the isolated Pt sites on PtGa/Al_2O_3 catalyst *via* silica coating layers for propane dehydrogenation at low temperature. Appl Catal B-Environ, 2022, 300: 120731
12 Srinath NV, Longo A, Poelman H, *et al. In situ* XAS/SAXS study of Al_2O_3-coated PtGa catalysts for propane dehydrogenation. ACS Catal, 2021, 11: 11320–11335
13 Rimaz S, Chen L, Monzón A, *et al.* Enhanced selectivity and stability of Pt-Ge/Al_2O_3 catalysts by Ca promotion in propane dehydrogenation. Chem Eng J, 2021, 405: 126656
14 Li J, Guan Q, Wu H, *et al.* Highly active and stable metal single-atom catalysts achieved by strong electronic metal-support interactions. J Am Chem Soc, 2019, 141: 14515–14519
15 He X, He Q, Deng Y, *et al.* A versatile route to fabricate single atom catalysts with high chemoselectivity and regioselectivity in hydrogenation. Nat Commun, 2019, 10: 3663
16 Xiong Y, Sun W, Han Y, *et al.* Cobalt single atom site catalysts with ultrahigh metal loading for enhanced aerobic oxidation of ethylbenzene. Nano Res, 2021, 14: 2418–2423
17 Qiao B, Wang A, Yang X, *et al.* Single-atom catalysis of CO oxidation using Pt_1/FeO_x. Nat Chem, 2011, 3: 634–641
18 Wang Y, Zheng Y, Han C, *et al.* Surface charge transfer doping for two-dimensional semiconductor-based electronic and optoelectronic devices. Nano Res, 2021, 14: 1682–1697
19 Jing H, Zhu P, Zheng X, *et al.* Theory-oriented screening and discovery of advanced energy transformation materials in electrocatalysis. Adv Powder Mater, 2022, 1: 100013
20 Han A, Wang X, Tang K, *et al.* An adjacent atomic platinum site enables single-atom iron with high oxygen reduction reaction performance. Angew Chem Intl Edit, 2021, 60: 19262–19271
21 Zhang B, Asakura H, Zhang J, *et al.* Stabilizing a platinum$_1$ single-atom catalyst on supported phosphomolybdic acid without compromising hydrogenation activity. Angew Chem, 2016, 128: 8459–8463
22 Tian S, Hu M, Xu Q, *et al.* Single-atom Fe with Fe_1N_3 structure showing superior performances for both hydrogenation and transfer hydrogenation of nitrobenzene. Sci China Mater, 2021, 64: 642–650
23 Zhang Z, Zhou M, Chen Y, *et al.* Pd single-atom monolithic catalyst: Functional 3D structure and unique chemical selectivity in hydrogenation reaction. Sci China Mater, 2021, 64: 1919–1929
24 Xu Q, Guo CX, Tian S, *et al.* Coordination structure dominated performance of single-atomic Pt catalyst for anti-Markovnikov hydroboration of alkenes. Sci China Mater, 2020, 63: 972–981
25 Furukawa S, Komatsu T. Intermetallic compounds: Promising inorganic materials for well-structured and electronically modified reaction environments for efficient catalysis. ACS Catal, 2017, 7: 735–765
26 H Sykes EC, Christopher P. Recent advances in single-atom catalysts and single-atom alloys: Opportunities for exploring the uncharted phase space in-between. Curr Opin Chem Eng, 2020, 29: 67–73
27 Thirumalai H, Kitchin JR. Investigating the reactivity of single atom alloys using density functional theory. Top Catal, 2018, 61: 462–474
28 Liu J, Lucci FR, Yang M, *et al.* Tackling CO poisoning with single-atom alloy catalysts. J Am Chem Soc, 2016, 138: 6396–6399
29 Hannagan RT, Giannakakis G, Flytzani-Stephanopoulos M, *et al.* Single-atom alloy catalysis. Chem Rev, 2020, 120: 12044–12088
30 Marcinkowski MD, Darby MT, Liu J, *et al.* Pt/Cu single-atom alloys as coke-resistant catalysts for efficient C–H activation. Nat Chem, 2018, 10: 325–332
31 Sun G, Zhao ZJ, Mu R, *et al.* Breaking the scaling relationship *via* thermally stable Pt/Cu single atom alloys for catalytic dehydrogenation. Nat Commun, 2018, 9: 4454
32 Cesar LG, Yang C, Lu Z, *et al.* Identification of a Pt_3 Co surface intermetallic alloy in Pt-Co propane dehydrogenation catalysts. ACS Catal, 2019, 9: 5231–5244
33 LiBretto NJ, Yang C, Ren Y, *et al.* Identification of surface structures in Pt_3Cr intermetallic nanocatalysts. Chem Mater, 2019, 31: 1597–1609
34 Wu Z, Wegener EC, Tseng HT, *et al.* Pd-In intermetallic alloy nanoparticles: Highly selective ethane dehydrogenation catalysts. Catal Sci Technol, 2016, 6: 6965–6976
35 Yang C, Wu Z, Zhang G, *et al.* Promotion of Pd nanoparticles by Fe and formation of a Pd_3Fe intermetallic alloy for propane dehydrogenation. Catal Today, 2019, 323: 123–128
36 Wong A, Liu Q, Griffin S, *et al.* Synthesis of ultrasmall, homogeneously alloyed, bimetallic nanoparticles on silica supports. Science, 2017, 358: 1427–1430
37 Grill C. Surface characterization of supported Pt-Pd bimetallic clusters using infrared spectroscopy. J Catal, 1981, 69: 454–464
38 Hippe C, Lamber R, Schulz-Ekloff G, *et al.* Influence of the strong metal-support interaction on the CO chemisorption at a Pt/SiO_2 catalyst. Catal Lett, 1997, 43: 195–199
39 Ertl G, Neumann M, Streit KM. Chemisorption of CO on the Pt(111) surface. Surf Sci, 1977, 64: 393–410
40 Lear T, Marshall R, Antonio Lopez-Sanchez J, *et al.* The application of infrared spectroscopy to probe the surface morphology of alumina-supported palladium catalysts. J Chem Phys, 2005, 123: 174706
41 Chen C, Sun M, Hu Z, *et al.* New insight into the enhanced catalytic performance of ZnPt/HZSM-5 catalysts for direct dehydrogenation of propane to propylene. Catal Sci Technol, 2019, 9: 1979–1988
42 Xie Z, Yan B, Lee JH, *et al.* Effects of oxide supports on the CO_2 reforming of ethane over Pt-Ni bimetallic catalysts. Appl Catal B-Environ, 2019, 245: 376–388
43 Li K, Chang Q, Yin J, *et al.* Deactivation of Pt/KL catalyst during n-heptane aromatization reaction. J Catal, 2018, 361: 193–203
44 Sattler JJHB, Ruiz-Martinez J, Santillan-Jimenez E, *et al.* Catalytic dehydrogenation of light alkanes on metals and metal oxides. Chem Rev, 2014, 114: 10613–10653
45 Cortright RD, Dumesic JA. Microcalorimetric, spectroscopic, and kinetic studies of silica supported Pt and Pt/Sn catalysts for isobutane dehydrogenation. J Catal, 1994, 148: 771–778
46 Cybulskis VJ, Bukowski BC, Tseng HT, *et al.* Zinc promotion of platinum for catalytic light alkane dehydrogenation: Insights into geometric and electronic effects. ACS Catal, 2017, 7: 4173–4181
47 Ruiz-Martínez J, Coloma F, Sepúlveda-Escribano A, *et al.* Effect of tin

content and reduction temperature on the catalytic behaviour of PtSn/TiO_2 catalysts in the vapour-phase hydrogenation of crotonaldehyde. Catal Today, 2008, 133-135: 35–41
48 Ruiz-Martínez J, Sepúlveda-Escribano A, Anderson JA, *et al.* Influence of the preparation method on the catalytic behaviour of PtSn/TiO_2 catalysts. Catal Today, 2007, 123: 235–244
49 Zhang B, Li G, Zhai Z, *et al.* PtZn intermetallic nanoalloy encapsulated in silicalite-1 for propane dehydrogenation. Aiche J, 2021, 67: 17295
50 Ryoo R, Kim J, Jo C, *et al.* Rare-earth-platinum alloy nanoparticles in mesoporous zeolite for catalysis. Nature, 2020, 585: 221–224

Acknowledgements This work was supported by the National Natural Science Foundation of China (22008135), and Beijing Municipal Science & Technology Commission (Z191100007219003). We thank the 1W1B station at Beijing Synchrotron Radiation Facility (BSRF) for collecting the XAFS data.

Author contributions Li Y conceived the idea and designed the research project; Ye C and Peng M collected and analyzed the data, and wrote the manuscript; Li Y and Chen C analyzed the propane dehydrogenation results; Wang D contributed to the characterizations of samples. All the authors commented on the manuscript and have given approval for the final version of the manuscript.

Conflict of interest The authors declare that they have no conflict of interest.

Supporting Information Experimental details and supporting data are available in the online version of the paper.

Chenliang Ye obtained his PhD degree in chemical engineering from Tianjin University in 2019. His research interests mainly focus on nano alloys and single atomic site catalysts, and he has expertise in controlled synthesis, advanced characterization and applications of catalytic materials for chemical transformations.

Mao Peng obtained his PhD degree in chemical engineering from Tianjin University in 2022. His research interests mainly focus on heterogeneous reaction engineering and theoretical research on energy catalysis.

Yadong Li received his BSc degree from the Department of Chemistry, Anhui Normal University in 1986 and his PhD degree from the Department of Chemistry, University of Science and Technology of China in 1998, under the supervision of Prof. Yitai Qian. He joined the faculty of the Department of Chemistry, Tsinghua University in 1999 as a full professor. His research interests focus on the synthesis, structure and applications of nanomaterials.

孤立Pt位点于Pt-Sn、Pt-Zn配位的PtSnZn有序金属间化合物选择性催化丙烷脱氢

叶陈良[1,2†], 彭茂[3†], 李杨[4], 王定胜[2], 陈晨[2], 李亚栋[2*]

摘要 随着页岩气的大规模开采, 丙烷脱氢制丙烯日益重要. 在本文中, 我们以Al_2O_3为载体, 结合强静电吸附法和程序升温还原法合成了~0.9 nm PtSnZn有序金属间化合物团簇(PtSnZn/Al_2O_3). PtSnZn金属间化合物的结构形成主要受动力学控制, Pt原子被Sn和Zn完全孤立, 形成Pt-Sn和Pt-Zn原子对. PtSnZn/Al_2O_3在丙烷脱氢反应中表现出优异的催化性能, 丙烯选择性高达~100%, 并且在长周期稳定性测试中丙烷转化率维持在40%以上. PtSnZn/Al_2O_3的丙烷脱氢催化性能远远优于Pt/Al_2O_3、PtSn/Al_2O_3和PtZn/Al_2O_3催化剂. 实验结果和理论计算表明, Sn 5p和Zn 4s与Pt 5d轨道的杂化使得Pt d带中心远离费米能级(−2.81 eV), 这在丙烷脱氢反应中会降低催化剂对丙烯的吸附能和抑制深度脱氢反应, 使得PtSnZn/Al_2O_3催化剂表现出高丙烯选择性和稳定性.

